Comprehensive Adaptive Tuning of Silicon RF Photonic Filters

Shengchang Cai, Gihoon Choo, Binhao Wang, Kamran Entesari, and Samuel Palermo

Department of Electrical and Computer Engineering
Texas A&M University, College Station, TX, USA 77843

***Abstract* — RF photonic filters are capable of achieving very high selectivity and dynamic tuning over multi-GHz ranges. This paper presents a mm-wave silicon photonic fourth-order tunable elliptic digital filter designed in the optical domain with ring-resonator-based all-pass filter (APF) unit cells. Inclusion of tunable phase shifters and Mach-Zehnder interferometer (MZI) couplers in the filter's rings and front-end provides comprehensive tuning to compensate for variations in ring resonance frequency, coupling ratio, and phase mismatches. A monitor-based adaptive tuning algorithm is proposed to calibrate the optical filter response with high accuracy.**

***Index Terms* — Adaptive tuning, integrated optics, optical filter, RF photonics, silicon photonics.**

I. Introduction

Applications such as wireless communications, radar, radio astronomy, and passive earth remote sensing can gain huge advantages from wideband multi-function transceivers. Given the instantaneous bandwidth of such a system, the role of receiver front-end filtering is critical to guarantee the necessary RF performance. This motivates the development of complex high-speed tunable filters with small form factors, which are not currently realizable with existing SAW [1] or MEMS [2] technologies. While integrated electrical SAW-less receivers which leverage a reciprocal passive mixing technique have been proposed for dynamic bandpass filtering [3], it is difficult to extend their operating frequency into the mm-wave range due to the requirement of a clock with a frequency at least 4X higher than the desired radio frequency.

RF photonics technology can enable widely tunable receivers with wide instantaneous bandwidth and dynamic filtering over a broad range of the spectrum [4]. Silicon photonics platforms, which offer compact low-loss waveguides and the ability to integrate many photonic circuits on a single die [5], offer the potential to enable chip-level realizations of these optical filters (Fig. 1).

However, the high-order photonic filters necessary in an RF system are sensitive to fabrication variations, necessitating the tuning of a significant number of photonic phase shifters to achieve the desired filter characteristics and/or reconfigure the filter. While manual tuning of high-order photonic filters has been demonstrated with the aid of external equipment [5], this is not feasible in production or operating environments.

This work was supported by the National Science Foundation under Grant EECS-1547432.

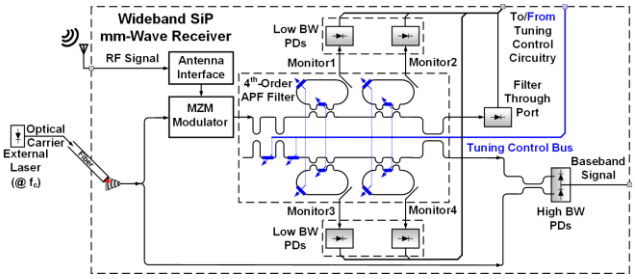

Fig. 1. Integrated silicon photonic mm-Wave receiver.

An interesting approach to tune high-order microring filters involves coupling a fraction of the output power for monitoring and utilizing an iterative algorithm for automatic resonance alignment [6]. While effective at fixing the center frequency, this method does not allow for any bandwidth control and requires excessive iterations. Another monitor-based adaptive tuning method which utilizes multiple calibration frequencies impressed upon the optical carrier with an input Mach-Zehnder Modulator (MZM) allows for control of both center frequency and bandwidth [7]. However, while this previous work compensated for filter ring resonance frequency variations, it failed to correct for coupler ratio imperfections which can dramatically affect filter selectivity.

This paper proposes a monitor-based adaptive tuning algorithm which extends the approach of [7] to compensate for coupling ratio variations and provide comprehensive tuning of an optical filter's response with high accuracy. The design of a tunable fourth-order elliptic optical filter is outlined in Section II. Section III presents the proposed comprehensive monitor-based adaptive filter tuning algorithm. Simulation results of optical filter calibration with the proposed tuning algorithm are presented in Section IV. Finally, Section V concludes the paper.

II. Optical Filter Design

To demonstrate the proposed tuning algorithm, a reconfigurable optical bandpass filter is first designed to have a 60GHz free spectral range (FSR) with a 5GHz passband from 32.5GHz to 57.5GHz and ~40dB stopband rejection with a 1550nm optical carrier.

Several approaches are possible to map the desired digital filter response to optical components, with a finite-

Optical Filter Coefficients

Ring	Ring Coupling Ratio κ_r (MZI Coupler)	Ring Phase Shift φ_r (rad)	Front-End Phase Shift φ_{fe} (rad)	Front-End Coupling Ratio κ_{fe}
1	0.3057	-3.2899	Up: -1.4028	0.5
2	0.1067	-2.8402		
3	0.3057	-2.9932	Dn: 1.4028	
4	0.1067	-3.4429		

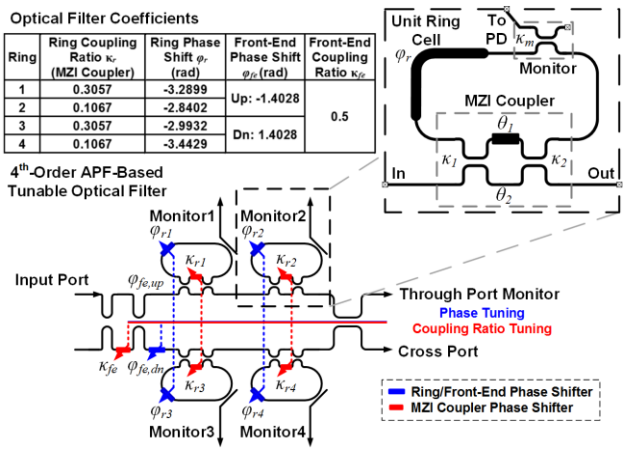

Fig. 2. Fourth-order APF tunable optical filter and optical coefficients.

impulse response (FIR) realized with a delay unit (optical phase shifter) and two directional couplers and an infinite-impulse response (IIR) generated with an optical ring resonator. Combining these structures allows for synthesis of any arbitrary digital filter response in the optical domain. Previously proposed implementations include structures based on waveguide grating routers [8], cascaded Mach-Zehnder interferometers (MZIs) [9], lattice structure filters [10], and all-pass filter (APF) unit cells [7]. However, waveguide grating router structures can only generate zeros and have limited tunability, while cascaded MZI topologies have inherently high loss. As a fourth-order APF-based structure has fewer phase shifters than a lattice structure, this topology is preferred for the proposed filter tuning algorithm.

As shown in Fig. 2, an APF-based implementation generates a complex conjugate response on the top/bottom arms with two 50% MZI/fixed couplers at the front/back end of the filter and two cascaded ring resonators. In the proposed filter, additional fixed and MZI couplers are added to each ring as monitors and coupling ratio tuning elements for the purpose of adaptive tuning. The desired digital filter transfer function is mapped to the optical components of the APF-based filter based on an all-pass decomposition algorithm, with the parameters summarized in Fig. 2 and the corresponding parametric filter response described by (1). Here c_r is the ring MZI coupler through port coefficient, c_m is the monitor coupler through port coefficient, c_{fe} and s_{fe} are the front-end MZI coupler through/cross port coefficients, r is the ring round trip loss, and φ_r is the ring phase shift.

Assuming 1dB ring round trip loss and a 10% monitor coupling ratio, Fig. 3 shows the filter output and monitor responses for a 50GHz center frequency relative to the 1550nm optical carrier. As shown in Fig. 4, the proposed optical APF-based filter has four pairs of zeros and poles that can be mapped exactly to that of the fourth-order elliptic digital filter.

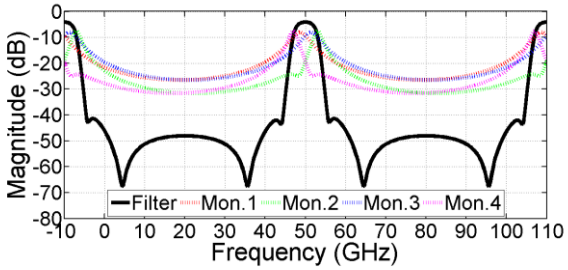

Fig. 3. Fourth-order optical filter and four monitor responses.

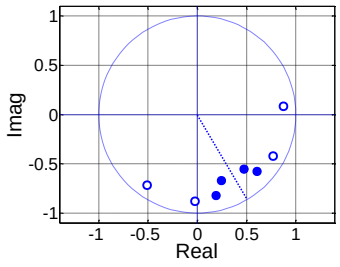

Fig. 4. Fourth-order optical filter z-plane plot.

III. Comprehensive Monitor-Based Filter Tuning

The proposed monitor-based adaptive tuning algorithm enables comprehensive filter calibration for ring resonance frequency, ring coupling ratio, and front-end phase mismatch and coupling ratio.

The optical filter proposed in Section II can be tuned by adjusting the pole/zero frequency and magnitude of each ring with phase shifters. In order to enable this, monitors are employed at each ring to extract ring response information. Each ring's monitor response is

$$H_m(z)=\frac{\left(s_1c_2e^{j\theta_1}+c_1s_2e^{j\theta_2}\right)s_m r e^{j\varphi_r}z^{-1}}{1+\left(s_1s_2e^{j\theta_1}-c_1c_2e^{j\theta_2}\right)c_m r e^{j\varphi_r}z^{-1}}, \qquad (2)$$

while the ring's through port response is

$$H_r(z)=\frac{\left(c_1c_2e^{j\theta_1}-s_1s_2e^{j\theta_2}\right)-e^{j(\theta_1+\theta_2)}c_m r e^{j\varphi_r}z^{-1}}{1+\left(s_1s_2e^{j\theta_1}-c_1c_2e^{j\theta_2}\right)c_m r e^{j\varphi_r}z^{-1}}, \qquad (3)$$

$c_{1,2}=\sqrt{1-\kappa_{1,2}}$, $s_{1,2}=\sqrt{\kappa_{1,2}}$, $c_m=\sqrt{1-\kappa_m}$, $s_m=\sqrt{\kappa_m}$.

where c_1, s_1, c_2, and s_2 are the cross/through port coefficients for the fixed 50% couplers in the ring MZI couplers, and θ_1 and θ_2 are the phase shift of the top/bottom arm of the MZI coupler, as shown in Fig. 2.

A. Resonance Frequency Tuning

From Eq. (2) and (3), both the monitor and ring response share the same pole location, whereas the ring through port response has an additional zero. Also note that the pole/zero from Eq. (3) always have the same phase independent of MZI coupler variation. As show in Fig. 5, the ring's resonance frequency aligns with the monitor's peak frequency when the pole and zero have the same phase. Therefore, the ring's resonance frequency can

$$H(z)=-\frac{j}{2}\left[c_{fe}e^{j\varphi_{fe,up}}\frac{\left(c_{r1}-c_{m1}r_1e^{j\varphi_{r1}}z^{-1}\right)\left(c_{r2}-c_{m2}r_2e^{j\varphi_{r2}}z^{-1}\right)}{\left(1-c_{r1}c_{m1}r_1e^{j\varphi_{r1}}z^{-1}\right)\left(1-c_{r2}c_{m2}r_2e^{j\varphi_{r2}}z^{-1}\right)}+js_{fe}e^{j\varphi_{fe,dn}}\frac{\left(c_{r3}-c_{m3}r_3e^{j\varphi_{r3}}z^{-1}\right)\left(c_{r4}-c_{m4}r_4e^{j\varphi_{r4}}z^{-1}\right)}{\left(1-c_{r3}c_{m3}r_3e^{j\varphi_{r3}}z^{-1}\right)\left(1-c_{r4}c_{m4}r_4e^{j\varphi_{r4}}z^{-1}\right)}\right] \qquad (1)$$

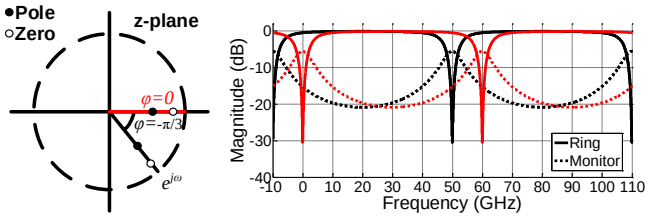

Fig. 5. Ring z-plane plot and ring/monitor response vs. ring phase shift.

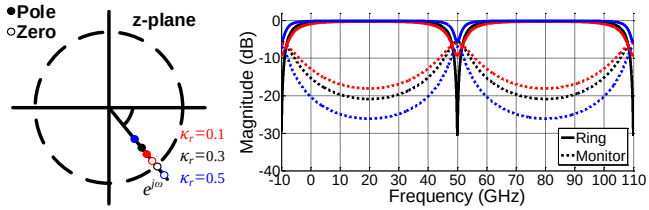

Fig. 6. Ring z-plane plot and ring/monitor response vs. ring coupling ratio.

be tuned to the desired frequency by adjusting the ring's phase shifter to maximize the power at the monitor port with the appropriate input stimulus frequency [7].

B. Ring Coupling Ratio Tuning

Fig. 6 shows how ring coupler ratio affects the pole/zero magnitude and thus the *Q* of the ring response. This can be calibrated by applying two tones: a ring's resonance frequency (ω_{res}) and an offset frequency ($\omega_{res}+\omega_{os}$) and calculating the magnitude ratio (*MR*)

$$MR = \left|\frac{H_m(\omega_{res})}{H_m(\omega_{res}+\omega_{os})}\right| = \frac{\sqrt{1-2R\cos\omega_{os}+R^2}}{1-R}, \qquad (4)$$

$$R = \left|c_m r\left(s_1 s_2 e^{j\theta_1} - c_1 c_2 e^{j\theta_2}\right)\right|,$$

where *R* is the pole magnitude. Given a specific pole magnitude *R*, the monitor magnitude ratio (*MR*) is well defined, as shown in Eq. (4). Therefore, to obtain the desired *MR*, pole magnitude *R* is calibrated by tuning the phase shifter θ in the MZI coupler.

C. Front-End Coupler/Phase Tuning

The front-end MZI coupler and phase shifter are implemented to balance the power and phase of the filter top/bottom paths. Notice from Fig. 3 that a null response exists when top/bottom arms are perfectly balanced. The filter out-of-band rejection is improved by maximizing the through-port monitor power at this null frequency [7] by adjusting the front-end MZI coupler and phase shifter.

D. Complete Filter Tuning Procedure

Fig. 7 shows the flow chart of the proposed filter tuning procedure with the stimulus frequencies for *fc*=50GHz. The coupling ratio calibration is carried out first for each ring with two calibration tones (52.95GHz and 47.05GHz), followed by ring resonance frequency tuning with four calibration stimuli (48.65GHz, 52.95GHz, 51.35GHz and 47.05GHz) applied at filter input, and

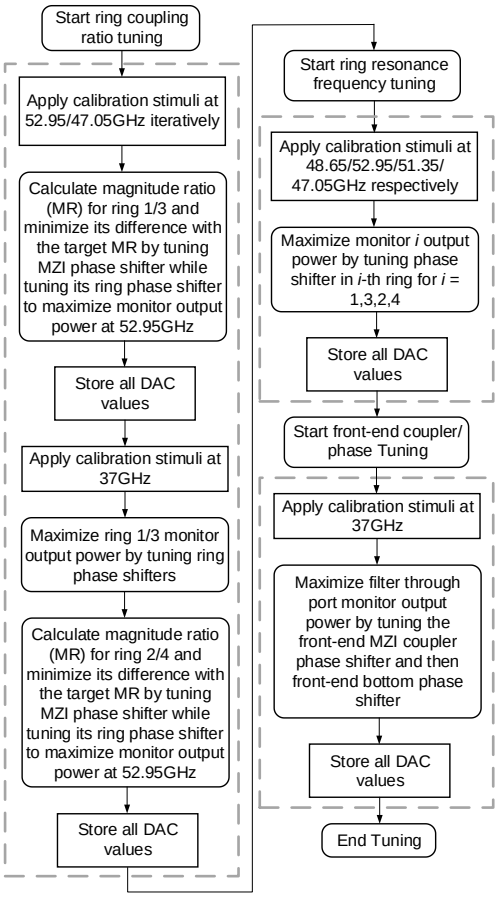

Fig. 7. Optical filter tuning flow chart for f_c=50GHz.

finally finished by front-end coupler/phase tuning with null frequency input stimulus (37GHz).

At each monitor port, a low-bandwidth photodetector (PD) and TIA are used to sense the average power level for comparison with a DAC-programmable reference level. This comparator output signal is digitally filtered by a tuning control finite-state machine (FSM) that adjusts the setting of the tuning DACs that drive the phase shifters. Once the maximum monitor power is obtained, the corresponding DAC code is stored.

IV. Simulation Results

The proposed filter tuning algorithm is simulated in MATLAB utilizing models for the proposed fourth-order elliptic optical filter, monitor port PD/TIAs, and the FSM which controls the DACs for adjusting the individual ring and top/bottom arm phase shifters. Key model parameters were extracted from simulations in Lumerical for the optical filter and COMSOL for the DAC control of the thermal resistors used to adjust the phase shifters. In the filter design, 1dB of ring round trip loss is accounted for and a 10% coupling ratio is used for each tuning monitor port.

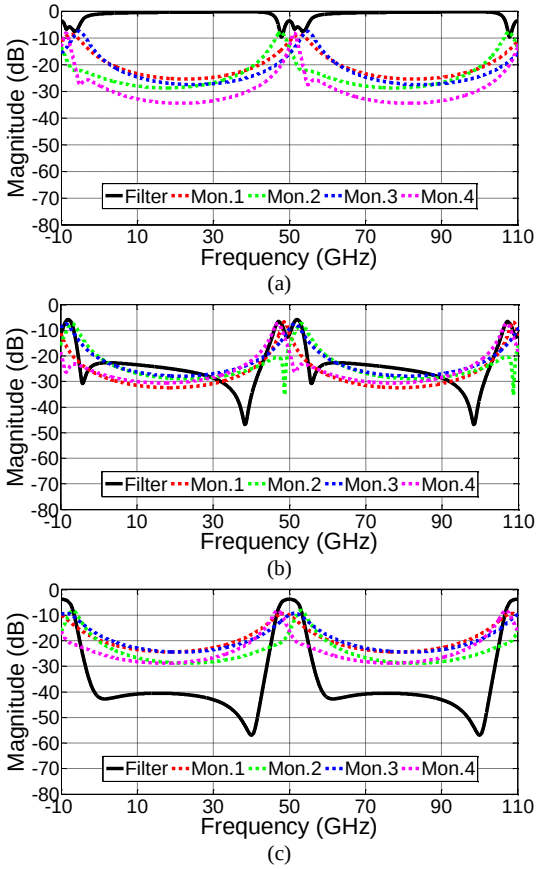

Fig. 8. Filter and monitor responses (a) before calibration, (b) after ring resonance/front-end phase mismatch calibration, and (c) w/ ring/front-end coupling ratio tuning.

In order to verify the proposed filter tuning algorithm, $\sigma=\pi/10$ for ring and front-end phase variation, $\sigma=0.13$ for all 50% coupler coupling ratio variation, $\sigma=0.01$ for all 10% coupler coupling ratio variation, and $\sigma=0.1$ for ring round trip loss variation is assumed [11]. Fig. 8 shows an example of the filter output and monitor port responses before and after the proposed adaptive tuning algorithm is applied to tune the filter to fc=50GHz. With the presence of coupling ratio variation, the filter response is still degraded even after the ring resonance/front-end phase mismatch calibration as shown in Fig. 8(b) and the filter response is able to achieve the target 5GHz bandwidth and ~40dB out-of-band rejection after applying ring/front-end coupling ratio calibration as shown in Fig. 8(c).

Monte Carlo simulations were then performed utilizing the same process variation data. As shown in Fig. 9, the pre-calibration filter performance distribution is poor, with a very wide variation in bandwidth and poor rejection. Excellent filter responses are obtained after applying the proposed tuning algorithm, with a $\pm 3\sigma$ range for bandwidth and out-of-band rejection of 4.75GHz/5.75GHz and 30dB/60dB, respectively.

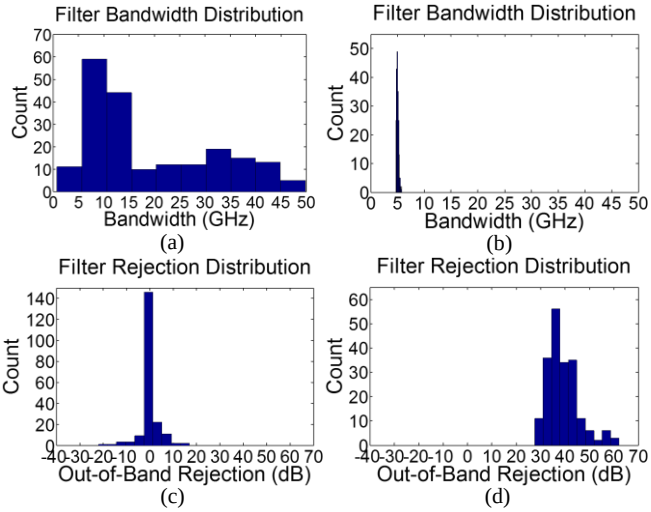

Fig. 9. Filter bandwidth distribution: (a) before calibration and (b) after calibration, rejection distribution: (c) before calibration and (d) after calibration.

V. Conclusion

This paper proposed a comprehensive adaptive tuning algorithm which allows for the automatic calibration of an optical filter response with high accuracy. Implementation of MZI couplers enable calibration of coupling ratio of ring/font-end couplers. Coupling ratio tuning together with ring resonance frequency and front-end coupler/phase tuning improves filter performance dramatically. The effectiveness of the proposed tuning algorithm is proved by Monte Carlo simulation with realistic process variation data.

References

[1] A. Safarian *et al.*, "Integrated blocker filtering RF front ends," *IEEE RFIC*, pp. 3-5, June 2007.

[2] K. Entesari *et al.*, "A 12–18 GHz three-pole RF MEMS tunable filter," *IEEE MTT*, vol. 53, no. 8, pp.2566–2571, 2005.

[3] H. Darabi *et al.*, "A blocker filtering technique for SAW-less wireless receivers," *IEEE JSSC*, vol. 42, no. 12, Dec. 2007.

[4] J. Rodgers, "Technologies for RF photonics in wideband multifunction systems", *IEEE AVFOP*, pp. 7-8, 2013.

[5] M. S. Rasras *et al.*, "Demonstration of a fourth-order pole-zero optical filter integrated using CMOS processes," *IEEE JLT*, vol. 25, no. 1, pp. 87–92, Jan. 2007.

[6] J. Mak *et al.*, "Automatic resonance alignment of high-order microring filter," *IEEE JQE*, vol. 51, no. 11, pp. 411, Oct. 2015.

[7] S. Cai *et al.*, "Adaptively-tunable RF photonic filters," *IEEE MWCAS*, pp. 1-4, Aug. 2015.

[8] K. Takada *et al.*, "1-GHz-spaced 16-channel arrayed-waveguide grating for a wavelength reference standard in DWDM network systems," *IEEE JLT*, vol. 20, no. 5, pp. 850-853, May 2002.

[9] N. Takato *et al.*, "Silica-based integrated optic Mach-Zehnder multi/demultiplexer family with channel spacing of 0.01-250 nm," *IEEE J-SAC*, vol. 8, no. 6, pp. 1120-1127, Aug. 1990.

[10] B. Guan *et al.*, "CMOS compatible reconfigurable silicon photonic lattice filters using cascaded unit cells for RF-photonic processing," *IEEE JSTQE*, vol. 20, no. 4, pp. 359-368, July/Aug. 2014.

[11] http://www.a-star.edu.sg/ime/RESEARCH/NANO-PHOTONICS-PROGRAMME/photonics_multiple_project_wafer_mpw_prototyping.aspx